Role of the Micro- and Nanostructure in the Performance of Surface-Enhanced Raman Scattering Substrates Assembled from Gold Nanoparticles

DANIEL M. KUNCICKY, STEVEN D. CHRISTESEN, and ORLIN D. VELEV*

Department of Chemical and Biomolecular Engineering, North Carolina State University, Raleigh, North Carolina 27695 (D.M.K., O.D.V.); and Edgewood Chemical Biological Center, U.S. Army RDECOM, Aberdeen Proving Ground-Edgewood Area, Maryland 21010 (S.D.C.)

Highly active and stable substrates for surface-enhanced Raman scattering (SERS) can be fabricated by using colloidal crystals to template gold nanoparticles into structured porous films. The structure-dependent performance of these SERS substrates was systematically characterized with cyanide in continuous flow microfluidic chambers. A matrix of experiments was designed to isolate the SERS contributions arising from nano- and microscale porosity, long-range ordering of the micropores, and the thickness of the nanoparticle layer. The SERS results were compared to the substrate structure observed by scanning electron microscopy (SEM) and optical microscopy to correlate substrate structure to SERS performance. The Raman peak intensity was consistently highest for nanoporous substrates with three-dimensionally ordered micropores, and decreases if the micropores are not ordered or not templated. Removing the nanoscale porosity by fusion of the nanoparticles (without removing the large micropores) leads to a drastic plunge in substrate performance. The peak intensity does not strongly correlate to the thickness of the nanoparticle films. The results make possible the efficient controlled fabrication of stable, reproducible, and highly active substrates for SERS based chemical sensors with continuous sampling.

Index Headings: **Surface-enhanced Raman spectroscopy; Colloidal crystal templating; Structured gold films; Cyanide detection; Nanoparticles.**

INTRODUCTION

Colloidal Au and Ag nanoparticles have been extensively studied as surface-enhancing Raman scattering (SERS) materials,[1,2] largely because they are easily prepared and yield a high Raman enhancement. The utility of this class of SERS materials for sensor applications and chemical assays can be limited by poor control over particle aggregation. This can lead to low reproducibility and variations of SERS intensities over time.[3,4] One route towards addressing these problems is to affix the nanoparticles onto a solid substrate. Controlled particle deposition onto solid substrates could prove to be one of the most promising and simple methods of forming surface-enhancing Raman scattering substrates.[5–16] Previously it has been shown that metallic nanoparticles adsorbed on a glass surface using either biospecific or metal-affinity interactions[5,6,9,13–16] could serve as SERS substrates. However, these two-dimensional (2D) nanoparticle layers are typically disordered and lack advanced features, such as long-range periodicity. Ordered arrays of separated Ag nanoparticles have been fabricated by evaporating metal through microsphere masks. This ''nanosphere lithography'' fabrication technique has yielded important data on the effect of particle size, shape, and ordering on the optical properties and SERS behavior.[17,18] Ordering and periodicity in substrates made by ''nanosphere lithography'' or microfabrication have been shown to improve the substrate performance.[19–22] In this study we compare various classes of SERS-active substrates with controlled structure assembled from gold nanoparticles. A key feature of these substrates is the high surface area imparted by multiple layers of aggregated gold nanoparticles combined with long-range and three-dimensional (3D) periodic ordering of pores in the substrate structure. This organized porosity may yield higher performance over 2D substrates.

The fabrication technique used has been developed as a result of our earlier research on nanostructures templated by colloidal crystals.[23–26] The gold nanoparticles in our method are mixed with sub-micrometer sized latex microspheres. The microspheres form long-range ordered 2D and 3D colloidal crystals when some of the water of the suspension is removed by filtration or drying. The gold nanoparticles are aggregated in the void spaces around the microspheres and form a structured metallic film that is preserved when the polymer template is dissolved. The method can be implemented in a continuous deposition process (Fig. 1), directly producing structured porous gold films that can serve as excellent substrates for SERS detection.[7,8,27] These substrates are made very easily, inexpensively, and without any complex equipment. They have high enhancement and, being made of chemically and physically inert gold, possess very good long-term stability.

Received 30 June 2004; accepted 21 December 2004.
* Author to whom correspondence should be sent. E-mail: odvelev@unity.ncsu.edu.

0003-7028/05/5904-0401$2.00/0

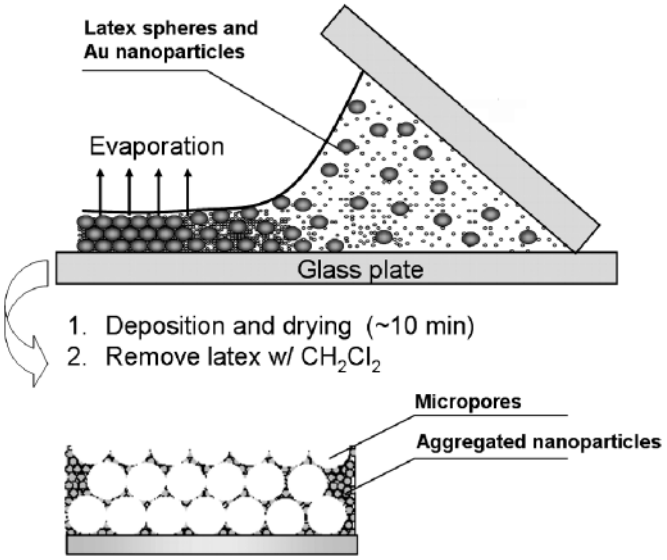

FIG. 1. Schematic of the one-step deposition of nanostructured substrates. The smaller gold nanoparticles are mixed with the larger latex microspheres and fill the void space in the colloidal crystal that forms by convective assembly in the drying region.

The nanoparticle substrates with controlled structure allowed us to perform continuous sampling experiments, where the metallic layers are encapsulated in a small chamber and their response is characterized in contact with the water solution of the analyte.[27] One very important feature of the substrate fabrication method is that it allows tuning the porosity on two hierarchical length scales. Large interconnected cavities are formed after the templating microspheres are removed. In addition, smaller pores are formed between the gold nanoparticles in the assembled structure; the size of these pores can be controlled by varying the diameter of the gold nanoparticles used in the process. While we proved that these substrates have excellent stability and high enhancement,[7,27] the effects of the structure and nano- and microporosity were not well understood. Characterizing and optimizing these parameters is the key to wider use of such substrates in chemical sensors and assays, and remains one of the largely unsolved problems in SERS. Such data could be instrumental in understanding in better depth the origin of the SERS effects and the factors that influence the substrate performance and sensitivity.

To systematically study the effect of substrate structure on SERS performance we designed a matrix of experiments that allowed us to isolate the individual contributions arising from gold nanoparticle loading, nanostructure, and microstructure. Three classes of SERS substrates were prepared and characterized in these experiments (Fig. 2):

(1) Substrates comprising multiple layers of aggregated gold nanoparticles without latex sphere templating, i.e., without templated microscale pores.
(2) Substrates in which microporosity has been added by templating the gold nanoparticles with micrometer-sized latex spheres. Both ordered arrays of latex spheres and randomly arranged latex spheres were compared in order to evaluate the role of the long-range micropore ordering on the substrate enhancement.
(3) Templated microporous substrates in which the nanoporosity has been reduced by heating the gold films to near the melting point of the nanoparticles in order to partially fuse them to each other. These substrates had the characteristic long-range organization of the micropores, but drastically reduced nanoporosity and surface area.

The performance of the SERS substrates was tested using a continuous water flux containing dilute sodium cyanide. Evaluating SERS performance in this way had two advantages: it simulated practical monitoring of water sources for defense, industrial, and environmental purposes, and it ensured a uniform cyanide surface concentration. Since the surface concentration was governed by

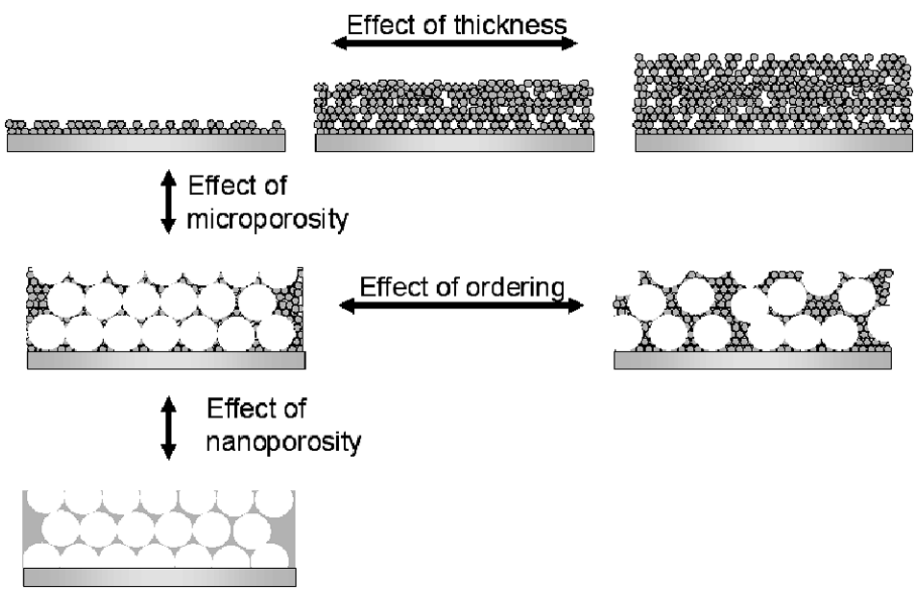

FIG. 2. Schematic of the types of SERS substrates used in the systematic investigation of the effect of gold nanoparticle loading and substrate nano- and microstructure on the SERS effectiveness.

thermodynamic equilibrium in the flowing liquid stream, the performance of the substrates was evaluated in terms of the structure-dependent behavior only. To achieve direct and reliable comparison of the various nanostructures shown in Fig. 2, multiple patches of SERS substrates were deposited on one microscope slide, and subsequently encapsulated into a single flow chamber. This allowed collecting spectra over multiple substrates in one experiment with minimal variances in the experimental conditions such as settings of laser power, solution composition, and ambient laboratory temperature. We collected multiple data points from randomly selected spots within the same substrate area, which allowed evaluating the variability of the substrate performance and reliability of the method.

EXPERIMENTAL

Materials. Sulfate-stabilized 650 nm latex microspheres (IDC, Portland, OR) were obtained at 3 wt % and were concentrated by gentle centrifugation to yield a ~20 wt % suspension. Aqueous suspensions of gold nanoparticles were synthesized using a standard citrate reduction protocol.[28] The nanoparticle size distribution was measured using scanning electron microscopy (SEM). The method typically produced gold nanoparticles that were 12 ± 2 nm. The gold particle suspension was concentrated to ~0.6 wt % by use of Centricon Plus-20 centrifugal filter units (Millipore, Billerica, MA). The suspensions were centrifuged at 1500×g for 10 min followed by an invert spin at 1100×g for 5 min to recover the retentate. In the final step, the gold suspension was concentrated to ~2 wt % via gentle centrifugation and mixed with pre-concentrated suspension of latex microspheres. The UV/Vis spectra of the gold suspension were measured before and after the concentration steps. There was no change in the position of the absorption peak at aproximately 520 nm. This confirmed that no significant changes in terms of aggregation or size distribution occurred due to the concentration of the nanoparticles. The SERS substrates were deposited onto standard 25 × 75 mm glass microscope slides (Fisher Scientific, PA). Prior to substrate deposition, the slides were cleaned in No-Chromix (Godax Laboratories, MD) for 12 h, thoroughly washed in deionized water using a Millipore RiOs 16 system, and oven dried at 70 °C. All chemicals were of certified ACS quality or better.

Surface-Enhanced Raman Scattering Substrate Deposition. The SERS substrates used in this study were fabricated by using the apparatus for continuous convective assembly designed by us earlier.[29] The substrates were deposited by entraining a small volume of particle suspension between two glass plates (Fig. 1). The top plate was attached to a linear motor and translated horizontally at a constant velocity (0.21–8.4 μm/s). Approximately 14 μL of concentrated gold suspension was used for non-templated substrates. A mixture of ≈14 μL of concentrated gold suspension and ≈7 μL of concentrated latex suspension was used for templated substrates. During templated substrate deposition the smaller gold nanoparticles aggregated in between the latex microspheres. After the templated films dried, the polystyrene latex template spheres were removed by submersing the substrate in methylene chloride (Fisher Scientific) for 15 min. In the final step, the substrates were treated with dimethylchlorosilane vapors (Sigma-Aldrich, St. Louis, MO) in a closed chamber for 15 min at 25 °C. This made the glass surface hydrophobic and improved the adhesion of the gold film, preventing it from peeling away in a flowing water stream. Since the van der Waals forces between metal particles of this size are quite strong, the upper layers of the nanoparticle aggregate substrates were stable in a flowing liquid stream. The stability was verified with scanning electron microscopy by viewing the SERS substrate structure before and after the flow-through experiments.

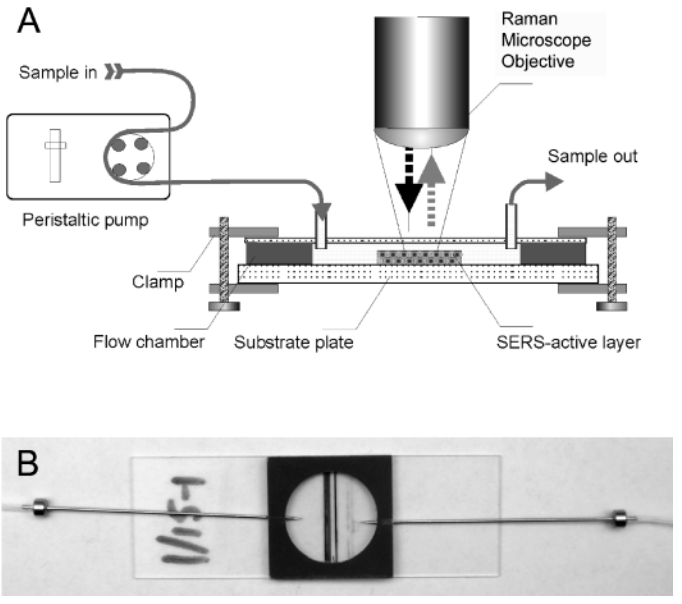

FIG. 3. (**A**) Schematic diagram of the experimental system used to evaluate the performance of SERS substrates. (**B**) Photograph of a typical microfluidic flow chamber (ported on two ends) containing SERS substrates.

Sample Preparation and Data Collection. The SERS substrates were encapsulated within a 630 μL, 2.0 mm deep, polycarbonate microscope chamber (Grace Biolabs, OR). The chamber was ported on two ends using syringe needles (Hamilton, NV) and connected to a variable flow peristaltic pump with Teflon tubing (Cole-Parmer, IL). The sample could be passed through the flow chamber at a rate of 0.2–1 mL/min. The SERS substrate and flow chamber were integrated with a Raman microscope (Fig. 3). An X-Y-Z translation stage was used to align the substrate at the focal plane of the microscope. The translation stage allowed us to position the excitation source at predetermined areas of the SERS substrate. This position was monitored and recorded with a charge-coupled device (CCD) camera. Results from two different Raman microscopes were collected and compared. The first system was a LabRam HR system (Jobin Yvon, NJ) with a 785 nm laser excitation source and a liquid N_2 cooled CCD detector. The second system was a Chromex Senturion (Bruker Optics, MA) with a 785 nm laser excitation source.

For both instruments, the laser power measured at the sample position was 1.0–2.0 mW and the data collection time was 30 or 45 s. Optical micrographs were acquired

with a BX61 optical microscope (Olympus, NY) equipped with a PDR-M81 digital camera (Toshiba, NY). Scanning electron microscopy (SEM) of the SERS substrates was performed with a F64 FESEM (JOEL, MA) at 5–10 kV accelerating voltage. UV/Vis spectroscopy was performed with a V550 UV-Vis spectrophotometer (Jasco, Japan).

Experimental Methodology. The Raman signal from nanostructured Au substrates is dependent on both the pH of the solution used to adsorb cyanide initially and on the pH of the solution, without cyanide, that was passed through the flow cell after initial cyanide absorption.[27] This provided the reasoning for measuring and comparing two classes of data, at high and low pH, for each substrate. In a typical experiment, deionized water was passed through the flow chamber for 10 min, and the background spectrum was collected. Then a solution of sodium cyanide in 0.1 M NaOH (Fisher Scientific) was passed through the flow chamber. In either case it took the signal about 10 min to reach steady state. Upon reaching steady state, spectra were collected at multiple positions on each SERS substrate. Then deionized water was passed through the flow chamber, and multiple spectra were again collected on each substrate. Using Grams/AI software (Thermogalactic, NH) the background spectrum obtained for water was subtracted from the spectra for sodium cyanide, and the peak area and height were determined.

RESULTS AND DISCUSSION

Surface-Enhanced Raman Scattering Substrate Structure Characteristics. Examples of the various types of structure that can be controllably imparted to the nanoparticle substrates are presented in Fig. 4. Microscale porosity is imparted to the gold substrates by templating the metallic nanoparticles around latex microspheres. These templated substrates have a hierarchical structure composed of aggregated gold nanoparticles arranged around micrometer-sized cavities. The type, quality, and structure of the template latex crystal is dependent on the deposition speed and latex suspension volume fraction.[29] By varying these parameters, we fabricated latex templates that were one, two, or three layers thick. Previously we showed that a polycrystalline structure consisting of hexagonal domains predominated in the latex crystal film.[29] Square arrays tended to form at grain boundaries and the edge transition between multilayers and monolayers; such transitions from multilayers to monolayers occur when the deposition speed is varied during the deposition process. However, when the latex microspheres and gold nanoparticles were mixed and deposited simultaneously the results were slightly different. In this case, the resulting latex sphere crystal structure was composed of a mixture of hexagonal and square crystal domains. The single crystal domain dimensions were in the 5–20 μm range (Figs. 4A and 4C–4E). In certain instances the packing of the latex spheres was random, resulting in no long-range crystal order (Figs. 4B and 4F). The reason for obtaining a disordered structure type is not well understood, but possibly results from the disrupting effect of the metal nanoparticles during the assembly.

The thickness of the templated substrate in these experiments was defined by the number of microsphere layers. The bilayer substrates templated with 650 nm microspheres were approximately 1 μm thick. The templated substrates (either ordered or disordered) span the entire width of the glass slide (2.5 cm) and typically occupy an area of 25–50 mm^2. When illuminated with white light at a small glancing angle, the ordered substrates produced a variety of intense colors due to Bragg diffraction (Fig. 4A). Based on this color diffraction, the ordered and disordered substrates were easily distinguished prior to measuring their SERS performance. After evaluating SERS performance in the continuous flow chamber, the substrates were characterized with SEM in order to verify the structure type and to observe the exact pore symmetry in the metallic films.

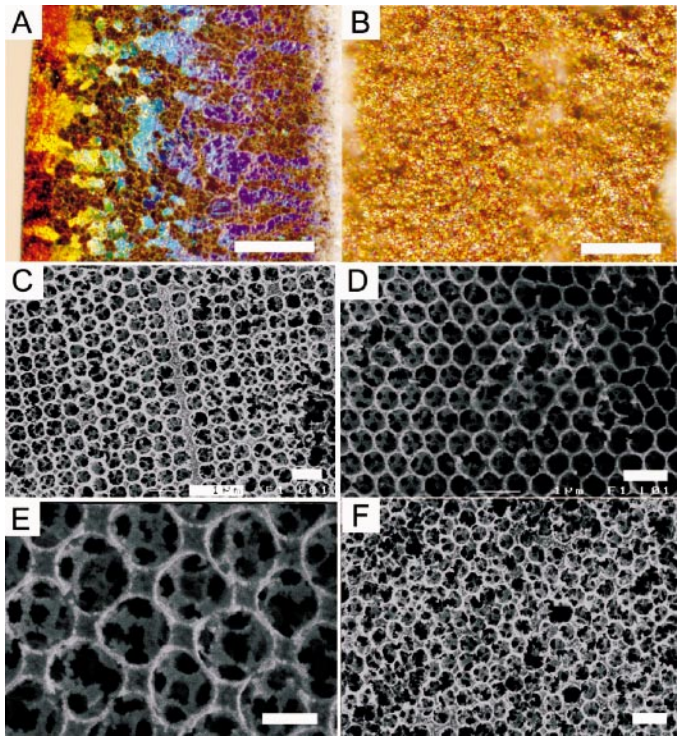

FIG. 4. Optical and SEM micrographs of different structures that can be created in the templated SERS substrates. (**A**) Ordered region at low magnification, optical microscopy. The colors come from the long-range ordered arrays; (**B**) disordered region at low magnification; (**C**) mixed bilayer at high magnification, SEM; (**D**) hexagonal bilayer at high magnification; (**E**) square bilayer; and (**F**) disordered region. The scale bars dimensions are: (A, B) 250 μm, (C, D, F) 1 μm, and (E) 500 nm.

The non-templated substrates, like the templated type, possess intrinsic nanoscale porosity imparted by aggregated nanoparticles. An important distinction is that the thickness of non-templated substrates can be finely tuned by controlling the deposition speed; more nanoparticle material is deposited in a given area at slower deposition speeds.[29] The thickness of non-templated substrates could be evaluated by comparing their relative transmission (Fig. 5A). The film thickness, L, was estimated using Eq. 1:

$$L = \frac{m}{\rho A}\frac{1}{1-\varepsilon} \quad (1)$$

The mass of gold in the film, m, is calculated from the original concentration of the gold suspension, ρ is the

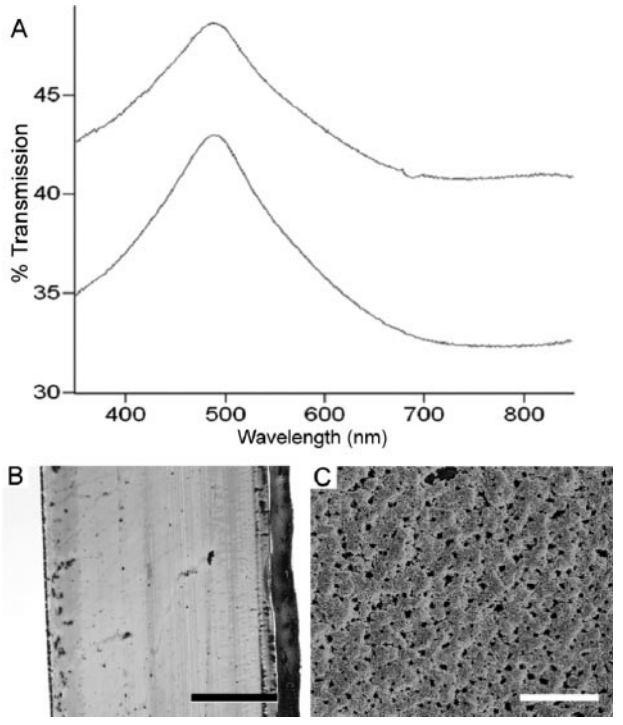

FIG. 5. (**A**) UV/VIS spectra showing the relative transmission for non-templated SERS substrates deposited at (***bottom***) 0.21 μm/s and (***top***) 0.84 μm/s. (**B**) Optical and, (**C**) SEM micrographs of non-templated SERS substrates. Scale bars in (B) and (C) are 10 mm and 5.0 μm, respectively.

gold density, ε is the void fraction for randomly packed spheres, and A is the measured film area. Based on Eq. 1, the average film thickness, L, ranged from 352 nm for a low deposition speed of 0.21 μm/s to 34.5 nm for a high deposition speed of 8.4 μm/s. These estimated values for the thickness are of the same order of magnitude as the empirical values independently measured by stylus profilometry. Despite the fact that the deposited film structure consisted of multiple layers of gold nanoparticles, a significant amount of light penetrated the film. Even for the thickest multilayer film that we could fabricate with our setup, over 30% of the light was transmitted in the SPR band at 720–780 nm (Fig. 5A). Micrometer-sized holes that penetrate the film were observed by SEM (Fig. 5C) and possibly contribute significantly to the optical transmission.

Effect of Substrate Structure on Surface-Enhanced Raman Scattering Response: Role of Nano- and Microporosity. A major finding of this work was that the SERS response of the aggregated nanoparticle substrates is strongly augmented with microsphere templating. We observed a multifold increase in the Raman signal for cyanide adsorbed on the templated gold substrates, relative to the non-templated type (Fig. 6). The substrates without any templating were only weakly enhancing, with a signal up to an order of magnitude lower than the structured templated ones. The SERS response of the disordered templated substrates was intermediate between the ordered templated substrate and the non-templated substrate. As reported in earlier studies,[27,30] the Raman signal increases when the pH of the solution surrounding the adsorbed cyanide is lowered, even when the low pH

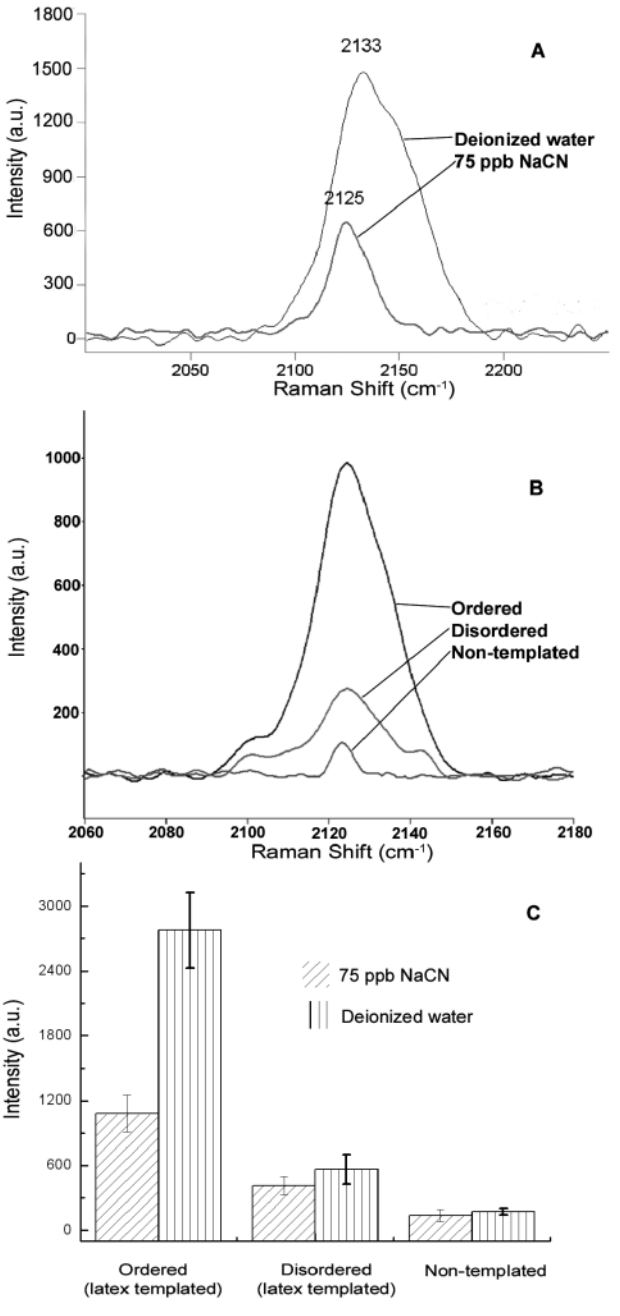

FIG. 6. (**A**) Characteristic sodium cyanide spectrum after 10 min of 75 ppb NaCN in 0.1 M NaOH (2125 cm^{-1}) and after subsequently passing deionized water through the flow cell (2133 cm^{-1}). (**B**) (***Top***) Characteristic sodium cyanide spectra for ordered latex-templated, (***middle***) disordered latex-templated, and (***bottom***) non-templated SERS substrates. (**C**) Averaged intensities of the 2125 cm^{-1} and the 2133 cm^{-1} peaks collected from each SERS substrate type (five data points from each substrate).

water phase contains no cyanide. The data presented here (Figs. 6A and 6C) confirm that this effect holds regardless of the substrate type. The results prove that the submicrometer pores left behind by the latex beads are contributing to the higher enhancement of our substrates and more, the long-range ordering of the pores is also a significant factor of SERS enhancement. These results also demonstrate that microsphere pore templating is one of the major ways to improve the sensitivity of SERS-based sensors.

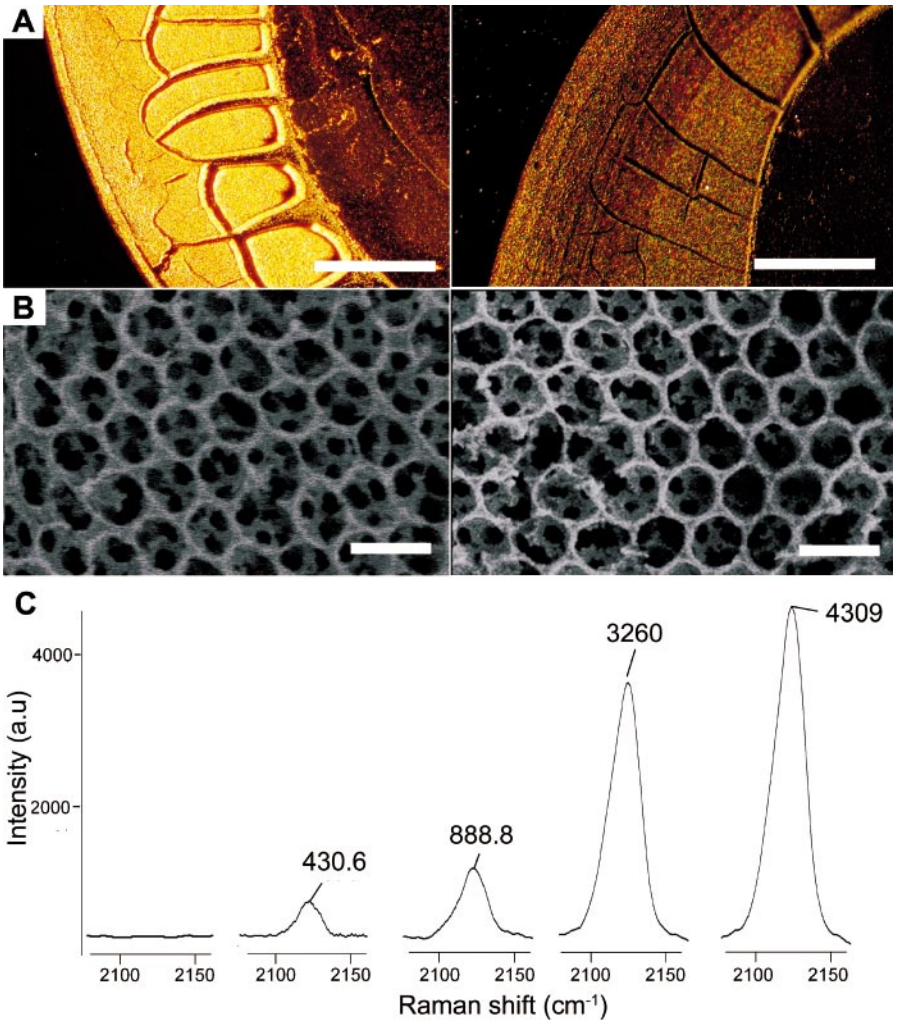

FIG. 7. (**Top**) Optical and (**bottom**) SEM micrographs of the SERS substrate (**A**) after and (**B**) before fusion of the Au nanoparticles. The SEMs show that the microscale features have been preserved. (**C**) Raman spectra of 150 ppb NaCN collected sequentially (shown from left to right) from the highly annealed end to the non-annealed end. The scale bar dimensions are (A) 1 mm, and (B) 1 μm.

The substrates that we study have very large surface area available for cyanide adsorption in comparison to microfabricated or vacuum deposited substrates. The major source of this surface area is the nanoscale porosity imparted by the aggregated nanoparticles. This specific area is not much affected by the presence of templated macropores. The nanoscale porosity can contribute to the SERS enhancement both by increasing the local intensity of the surface plasmons in between the gaps[31–33] and by allowing more analyte to adsorb per unit surface of the substrate. The next major goal of this study was to understand the relationship between nanoporosity and SERS performance. In order to characterize this parameter, we managed to remove much of the nanoporosity by controlled low-temperature fusion, while preserving the microscale porosity imparted by the latex templates. The elimination of the nanopores was accomplished by heating the templated substrates near the fusing point of the gold nanoparticles. Although the melting temperature of bulk gold is ~1064 °C, it is well known that gold nanoparticles melt at much lower temperatures due to the thermodynamic implications of their high surface area to volume ratio.[34–38]

The nanoparticles can thus easily be fused by flame-treating the templated gold substrates with a Bunsen burner. After annealing for 30 s, the substrate color changed from brownish-red to the color of bulk gold (Fig. 7A). Additional evidence for particle fusion was shown by the extreme broadening of the surface plasmon resonance (SPR) peak centered on 780 nm, which indicates the formation of large continuous metal domains. Visual examination of the metal films still revealed the Bragg diffraction colors, showing that the large-scale arrays of large micropores were preserved. We also examined the flame-treated substrates with scanning electron microscopy (SEM) (Fig. 7B) and verified that the microscale ordered pores were retained. No new background Raman bands appeared after the fusion experiments, indicating that surface contamination had not occurred during the heat annealing.

We were able to make single samples with a gradient of the nanoporosity, where the nanoparticles are all fused on one end and unchanged on the other. The experiment of reducing nanoscale porosity by partial fusion was designed to collect and compare data from the same flow chamber and from the same substrate. This was done by imposing a steep temperature gradient on the substrates. The thermal gradient was imposed on the back side of

one of the SERS substrates by holding the substrate at a 45 degree angle over a Bunsen burner so one side of the substrate is heated while the other remains cold. This technique produced substrates that were highly annealed at one end and only partially annealed at the other. The spatial dependence was expressed by the gradual color change from golden at one end to reddish-brown at the other (Fig. 7A).

The SERS cyanide peaks obtained by scanning the response of areas with different degrees of fusing are shown in Fig. 7C. Raman signal from the completely fused substrates was not observed under these conditions. A small peak appeared and increased as spectra were collected from less and less heated areas, and it reached its normal height in the non-modified side of the substrate. These data convincingly demonstrate that nanoporosity on the size scale of the particles is a key factor directly related to high SERS performance. It may be expected that substrates with high surface roughness imparted by the nanoparticles generate stronger plasmon resonances. This, however, may not be the major effect here, as the surface plasmon intensity in a continuous metal structure (i.e., the fully annealed case) is modulated by features comparable to the wavelength of light and is not affected too much by nanoscale features.[39,40] Our working hypothesis is that the large SERS signal collected from the nanoporous substrates is more closely correlated to the large surface area. This large surface area allows more cyanide to adsorb from the surrounding solution. In summary, this cycle of experiments proved that both the micro- and the nanopores contribute to the high enhancement of our substrates, but the nanopores are the ones leading to the key effect, possibly mostly due to the high surface area available for analyte adsorption.

Reproducibility of the Raman Signal from Different Substrates. Surface-enhanced Raman scattering has been proven to be a method with high sensitivity, but so far attempts to market practical SERS-based detection devices and assays have had limited success. One of the major reasons for this is the lack of standardized substrates that would have uniform and reproducible SERS performance on any equipment. The existence of ''hot'' and correspondingly ''cold'' spots on the surface of some substrates is interesting for understanding the fundamentals of the enhancement effects, but could be a major impediment in the practical application of the substrates,[41,42] where alignment and optimization is typically not possible. The use of silver could also be a source of poor reproducibility due to contamination and oxidation of the metal surface.

The substrates made from assemblies of gold nanoparticles promise to have stable and uniform performance. In order to estimate reproducibility, we compared the absolute peak intensity obtained on different substrates that we had analyzed during this study. The data were compiled from experiments performed on four substrates over a 12-month period. The experiments had been conducted using the same laser power and collection time. The reproducibility of the signal was evaluated by comparing the peak height for the 2125 cm^{-1} SERS band of 75 ppb NaCN. Between two and five data points were collected from each substrate. The results are plotted as histograms in Fig. 8.

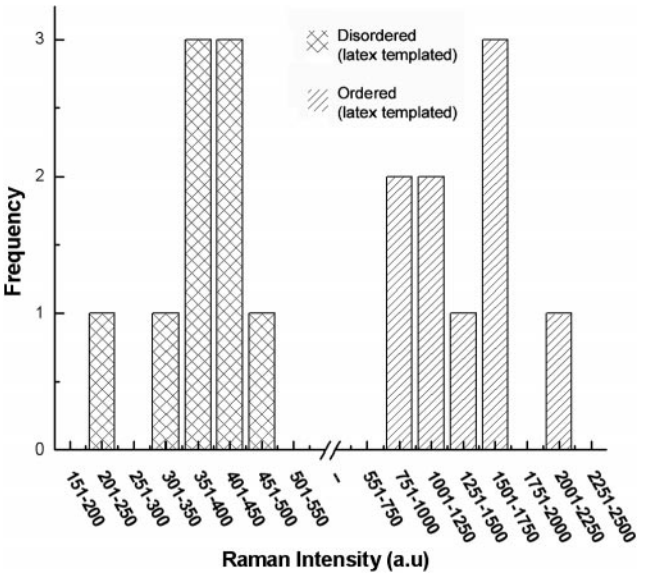

FIG. 8. Distribution of Raman intensity data for disordered and ordered templated substrates (compare with Fig. 6). The data scattering was 25% for the ordered templated substrate and 17% for the disordered templated substrate.

The ordered templated substrates consistently produced a signal better than approximately 750 a.u., even after an arbitrary storage time, and at any area sampled. The performance of the disordered templated substrates was worse in terms of intensity, yet the scattering of the data values was about the same. These data again demonstrate that the long range ordering of the micropores is conducive to achieving a high signal. The results point out that the templated substrates are likely to have the reproducibility, stability, and high enhancement required for practical application in routine SERS analysis and chemical detection of cyanide. A study of the functionalization of such substrates for the detection of a wide range of other analytes is under way.

Effect of Gold Nanoparticle Surface Loading. The quantity of metallic gold required for making these substrates is rather small. The optimization of substrate performance and cost of fabrication, however, required understanding the correlation between the amount of metal nanoparticles deposited per unit area and the strength of the SERS signal. A major advantage of the convective assembly technique is that it allowed us to easily control the film thickness by varying the deposition speed. To characterize the effect of film thickness, we compared the sodium cyanide peak intensity for substrates with different thicknesses. These experiments were performed on non-templated gold substrates rather than with templated ones, as the structure of the large pores in the templating multilayer colloidal sphere crystals changes with thickness.[29]

The results of these SERS experiments are shown in Fig. 9. Although the non-templated substrates have much lower Raman signal than the templated ones (compare with Fig. 6) spectra were reliably registered in some of the areas studied. Between 40 and 60% of the spots analyzed produced poor spectra. These ''cold spots'' are probably smooth, well-packed nanoparticle layers, where macroscale surface roughness is low. All data points of

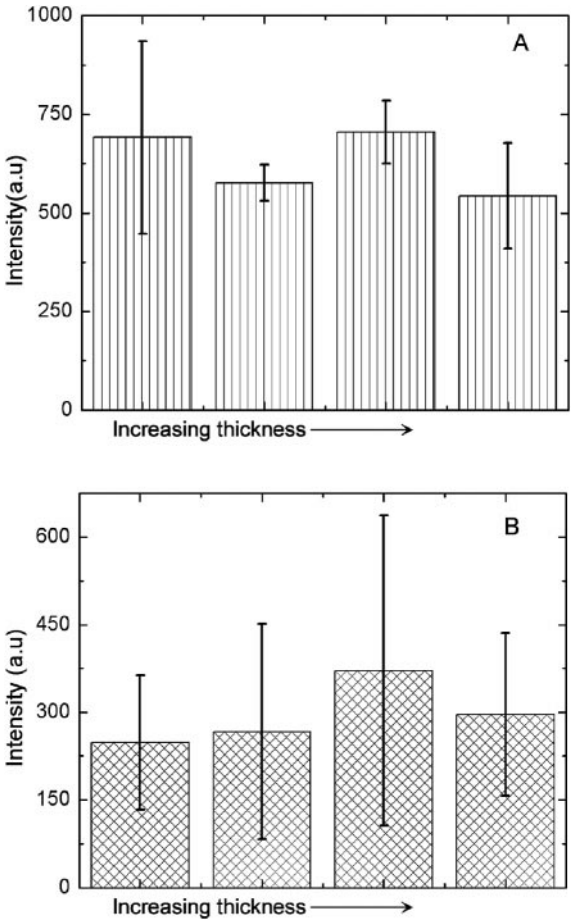

FIG. 9. Averaged 150 ppb cyanide peak intensity for SERS substrates with different thicknesses at (**A**) high pH and (**B**) low pH. No clear trend in SERS activity based on substrate thickness can be distinguished.

signal-to-noise ratio less than 3 were discarded and are not represented in Fig. 9. The averaged peak intensity data for the ''hot spots'' in substrates with increasing thickness vary from sample to sample, but the lack of clear trend points out that there was no strong correlation between gold particle loading and Raman intensity (Fig. 9). This is a surprising result with important practical consequences. The most probable explanation is that because of the attenuation of the excitation light beam by the metallic gold, the SERS enhancement occurs only in the thin topmost layer of gold nanoparticles and the number of underlying gold layers does not affect the result significantly. The practical significance of this result is that only a relatively thin layer of tens of nanometers of gold is required to generate a strong signal and thus the amount of gold nanoparticles deposited onto the surface can be reduced without significant degradation of the substrate quality. The same conclusions are possibly also valid for templated porous substrates (resulting in an optimal thickness of approximately two layers of pores), but direct experimental verification in this case is more difficult.

CONCLUSION

The fabrication of substrates with reliable and consistent performance is the key to using SERS in sensors, water quality monitors, and routine analytical practice. This problem is more difficult to address for substrates made by nanoparticle self-assembly, as the number of parameters involved in the fabrication is much larger and the control of these parameters can be complicated. The results presented here demonstrate that the combination of convective assembly and latex templating in our continuous deposition setup allows ''engineered'' fabrication of substrates with consistently high and reproducible enhancements. More importantly, the systematic data clearly point out the various sources of Raman enhancement in our experiments.

The first source of enhancement is the micropores templated by the latex spheres. This can be anticipated, having in mind that the size of these pores (typically 650 nm) is comparable to the wavelength of the excitation laser beam. Optimization of the size of the pores (which can be adjusted via the size of the microsphere templates) was not performed, but this could increase the substrate efficiency further. We observed that the long-range organization of the pore arrays in hexagonal and square symmetry also contributes to the strength of the enhancement; stronger signals are observed when the pores are periodically organized. This effect has been reported previously with microfabricated substrates,[21] but we are the first to observe it with self-assembled nanoparticle substrates. The effect possibly originates from long-range resonance of the light and plasmons within the aligned spherical cavities (broadly similar to diffraction resonance phenomena). Theoretical understanding of this phenomenon could lead to interesting insights on the microphotonic properties of the substrates.

The results also prove that the nanoscale porosity is an even more significant factor in the electromagnetic enhancement. Elimination of the nanoporous component imparted by the aggregated gold nanoparticles completely eliminates the signal under the conditions tested here. Research on evaporated silver films has shown that adsorbate molecules residing in the nanopores provide the predominate contribution to the enhanced Raman signal.[43,44] Our results confirm the earlier results on the importance of nanoporosity. We believe that the very high surface area of aggregated particle substrates (compared to alternative structures made by vacuum metal deposition) provides additional increase of the Raman signal intensity due to the larger amount of cyanide adsorbed, but possibly also due to the higher surface roughness. The nanoparticle assembly technique is not only simple, but creates SERS substrates with very high surface area that largely improves detection sensitivity. We have also shown that the thickness of the substrates is not a major factor contributing to their performance, so we can use only very thin layers of templated gold nanoparticles. These results are a step towards the engineered fabrication of self-assembled substrates that are optimized in their structure, performance, stability, and cost of fabrication.

ACKNOWLEDGMENTS

We are grateful to Dwight Walker (Glaxo Smith Kline) and Stefan Franzen for experimental assistance, use of equipment, and enlightening discussions. We would also like to acknowledge Derek Brown, Brian Prevo, Kristina Gonser, and Jason Guicheteau for their contributions

and assistance. This study was supported by the Army Research Office (DAAD19-02-1-0287).

1. C. G. Blatchford, J. R. Campbell, and J. A. Creighton, Surf. Sci. **120,** 435 (1982).
2. O. Siiman, L. A. Bumm, R. Callaghan, C. G. Blatchford, and M. Kerker, J. Phys. Chem. **87,** 1014 (1983).
3. R. Montes, C. Contreras, A. Ruperez, and J. J. Laserna, Anal. Chem. **64,** 2715 (1992).
4. P. A. Schueler, J. T. Ives, F. Delacroix, W. B. Lacy, P. A. Becker, J. M. Li, K. D. Caldwell, B. Drake, and J. M. Harris, Anal. Chem. **65,** 3177 (1993).
5. K. C. Grabar, R. G. Freeman, M. B. Hommer, and M. J. Natan, Anal. Chem. **67,** 735 (1995).
6. R. G. Freeman, K. C. Grabar, K. J. Allison, R. M. Bright, J. A. Davis, A. P. Guthrie, M. B. Hommer, M. A. Jackson, P. C. Smith, D. G. Walter, and M. J. Natan, Science (Washington, D.C.) **267,** 1629 (1995).
7. P. Tessier, O. D. Velev, A. T. Kalambur, A. M. Lenhoff, J. F. Rabolt, and E. W. Kaler, Adv. Mater. **13,** 396 (2001).
8. P. M. Tessier, O. D. Velev, A. T. Kalambur, J. F. Rabolt, A. M. Lenhoff, and E. W. Kaler, J. Am. Chem. Soc. **122,** 9554 (2000).
9. R. G. Freeman, M. B. Hommer, K. C. Grabar, M. A. Jackson, and M. J. Natan, J. Phys. Chem. **100,** 718 (1996).
10. L. A. Lyon, C. D. Keating, A. P. Fox, B. E. Baker, L. He, S. R. Nicewarner, S. P. Mulvaney, and M. J. Natan, Anal. Chem. **70,** 341R (1998).
11. C. H. Munro, W. E. Smith, M. Garner, J. Clarkson, and P. C. White, Langmuir **11,** 3712 (1995).
12. X. M. Dou and Y. Ozaki, Rev. Anal. Chem. **18,** 285 (1999).
13. S. P. Mulvaney, L. He, M. J. Natan, and C. D. Keating, J. Raman Spectrosc. **34,** 163 (2003).
14. A. Wei, B. Kim, B. Sadtler, and S. L. Tripp, Chem. Phys. Chem. **2,** 743 (2001).
15. J. Wang, T. Zhu, J. Q. Song, and Z. F. Liu, Thin Solid Films **329,** 591 (1998).
16. G. Bar, S. Rubin, R. W. Cutts, T. N. Taylor, and T. A. Zawodzinski, Langmuir **12,** 1172 (1996).
17. C. L. Haynes and R. P. Van Duyne, J. Phys. Chem. B **105,** 5599 (2001).
18. C. L. Haynes and R. P. Van Duyne, J. Phys. Chem. B **107,** 7426 (2003).
19. R. L. Moody, T. Vo-Dinh, and W. H. Fletcher, Appl. Spectrosc. **41,** 966 (1987).
20. J. C. Hulteen and R. P. Van Duyne, J. Vac. Sci. Technol. A **13,** 1553 (1995).
21. M. Kahl, E. Voges, S. Kostrewa, C. Viets, and W. Hill, Sens. Actuators, B **51,** 285 (1998).
22. R. P. Van Duyne, J. C. Hulteen, and D. A. Treichel, J. Chem. Phys. **99,** 2101 (1993).
23. O. D. Velev, P. M. Tessier, A. M. Lenhoff, and E. W. Kaler, Nature (London) **401,** 548 (1999).
24. O. D. Velev and E. W. Kaler, Adv. Mater. **12,** 531 (2000).
25. O. D. Velev, T. A. Jede, R. F. Lobo, and A. M. Lenhoff, Nature (London) **389,** 447 (1997).
26. O. D. Velev and A. M. Lenhoff, Curr. Opin. Colloid Interface Sci. **5,** 56 (2000).
27. P. M. Tessier, S. D. Christesen, K. K. Ong, E. M. Clemente, A. M. Lenhoff, E. W. Kaler, and O. D. Velev, Appl. Spectrosc. **56,** 1524 (2002).
28. J. W. Slot and H. J. Geuze, Eur. J. Cell Biol. **38,** 87 (1985).
29. B. G. Prevo and O. D. Velev, Langmuir **20,** 2099 (2004).
30. R. D. Shelton, J. W. Haas, and E. A. Wachter, Appl. Spectrosc. **48,** 1007 (1994).
31. M. Moskovits, J. Chem. Phys. **69,** 4159 (1978).
32. N. Liver, A. Nitzan, and J. I. Gersten, Chem. Phys. Lett. **111,** 449 (1984).
33. P. K. Aravind, A. Nitzan, and H. Metiu, Surf. Sci. **110,** 189 (1981).
34. P. Buffat and J. P. Borel, Phys. Rev. A **13,** 2287 (1976).
35. J. P. Borel, Surf. Sci. **106,** 1 (1981).
36. J. Ross and R. P. Andres, Surf. Sci. **106,** 11 (1981).
37. T. Castro, R. Reifenberger, E. Choi, and R. P. Andres, Phys. Rev. B **42,** 8548 (1990).
38. T. E. Daubert and R. P. Danner, Eds., *Data Compilation Tables of Properties of Pure Compounds* (Design Institute for Physical Property Data, American Institute of Chemical Engineers, New York, 1985), vol. 1.
39. J. A. Creighton, C. G. Blatchford, and M. G. Albrecht, J. Chem. Soc. Faraday Trans. **75,** 790 (1979).
40. F. J. Garcia-Vidal and J. B. Pendry, Phys. Rev. Lett. **77,** 1163 (1996).
41. T. Vo-Dinh, M. Y. K. Hiromoto, G. M. Begun, and R. L. Moody, Anal. Chem. **56,** 1667 (1984).
42. E. J. Zeman and G. C. Schatz, J. Phys. Chem. **91,** 634 (1987).
43. E. V. Albano, S. Daiser, G. Ertl, R. Miranda, K. Wandelt, and N. Garcia, Phys. Rev. Lett. **51,** 2314 (1983).
44. C. A. Murray and S. Bodoff, Phys. Rev. B **32,** 671 (1985).